Optics and Lasers in Engineering 106 (2018) 24–31

Contents lists available at ScienceDirect

Optics and Lasers in Engineering

journal homepage: www.elsevier.com/locate/optlaseng

A systematic analysis for the quantitative comparison of phase retrieval methods based on alternating projections

Francisco E. Veiras[a,*], Arturo Bianchetti[b], Pablo Etchepareborda[c], Ana L. Vadnjal[c], Alejandro Federico[b]

[a] Universidad de Buenos Aires, Facultad de Ingeniería, Departamento de Física, GLOmAe. CONICET., Buenos Aires C1063ACV, Argentina
[b] Electrónica e Informática, Instituto Nacional de Tecnología Industrial, P.O. Box B1650WAB, San Martín B1650KNA, Argentina
[c] Electrónica e Informática, Instituto Nacional de Tecnología Industrial, CONICET, P.O. Box B1650WAB San Martín B1650KNA, Argentina

ARTICLE INFO

Keywords:
Phase retrieval
Metrological instrumentation
Computation methods

ABSTRACT

We present a numerical and experimental scheme for the systematic analysis and comparison of phase retrieval techniques based on alternating projection numerical methods. This comparison allows us to evaluate the most common and recently introduced phase retrieval methods. The proposed scheme gives a quantitative comparison that helps to elucidate the differences between them and develop proper technical implementations of phase retrieval. The comparison is made by means of a numerical and experimental scheme that allows us to evaluate phase retrieval experiments. In this work, the drawbacks of using arbitrary random initial seeds to support the phase retrieval numerical algorithms are also analyzed and discussed. Moreover, we show the convenience of using a rough object phase estimation, which is obtained by means of a simple holographic technique, as the initial seed. This seed dramatically reduces the computational load of the algorithms by decreasing the successive iterations from hundreds to less than twenty. The experimental object under study is a random phase object within a micro-channel. As a proof of concept, this micro-channel combined with a millimeter size semicircular hole, which provides a reference wave, conforms a primitive sensor. The performance of the algorithms is not only measured by the usual convergence error, but also by means of a quality index that requires a direct comparison against the generally unknown original phase object. Thus, in order to evaluate the experimental performance of the phase retrieval techniques, we implement an interferometric optical setup that allows us to compare the results obtained by both techniques. The experiment proposed is a valuable tool for quantitative experimental evaluation of phase retrieval techniques in the optical domain.

1. Introduction

Phase retrieval techniques are particularly used in different fields such as electron microscopy, X–ray crystallography and astronomy. Moreover, there are a variety of phase retrieval techniques. Some of them introduce changes in the recording scheme such as changing wavelengths, changing the distance between the sample and the sensor or the distance between the illumination source and the sample, or moving the illumination laterally across the sensor (ptychography) and illuminating the sample from different directions (Fourier-ptychography). As is very well known, this problem plays a central role in various fields of science and engineering when it is investigated from a more general point of view. In this work, we avoid the use of interferometric setups or recently introduced multi-image approaches [1,2]. A contemporary overview of the phase retrieval problem with application to optical imaging should be consulted in Ref. [3] with an exhaustive list of references therein. Interested readers can find in this review links between relevant optical physics and signal processing methods and algorithms.

We focus on phase retrieval techniques based on alternating projection numerical methods. This approach only requires knowing the Fourier magnitude and the support of the tested object. Therefore, it is very attractive for the development of refractive sensors since the complexity level of the optical setup is reduced. However, these recursive numerical methods either fail to work or show partial results that are difficult to interpret. A reason to explain this difficulty is that there is no guarantee that a solution can be found algorithmically. This problem is not convex, and the solution depends on the initialization and the complex object signal. Therefore, it is convenient to carry out theoretical and experimental comparisons between the well-known recursive algorithms based on a proper object signal as a standard for analysis. To our knowledge, this kind of comparisons cannot be found in the relevant lit-

* Corresponding author.
E-mail address: fveiras@fi.uba.ar (F.E. Veiras).

https://doi.org/10.1016/j.optlaseng.2018.02.005
Received 20 December 2017; Received in revised form 9 February 2018; Accepted 11 February 2018
0143-8166/

erature. Moreover, we could not find a quantitative comparison of the retrieved phase against the object optical phase.

With the name of *Optical Phase Retrieval* (OPR), we refer to the classic problem that can be shortly described as the reconstruction of an object signal $g_o \in \mathbb{C}$ from the magnitude of its Fourier transform $F = \mathcal{F}(g_o)$. OPR is formulated as the empirical risk minimization expressed by the following equation:

$$\hat{g} = min_{\{g\}} \sum_{k,l=1}^{2M} [|F_{k,l}|^2 - | < a_{k,l}, g > |^2]^2, \tag{1}$$

where $\hat{g} \in \mathbb{C}^{2N \times 2N}$ is the complex object function to be recovered given the intensity measurements $|F| \in \mathbb{R}_+^{2M \times 2M}$. $< a_{k,l}, \cdot >$ denotes the decomposition in vectors $a_{k,l}$ of the Fourier basis being $M > 2N - 1$ and adopting a frame of work based on the oversampled discrete Fourier transform (zero padding for the object function and oversampling by 2 or more). From the analysis of Eq. (1), it is not clear how to find a global minimum, even if one exists. In addition, it should be noted that all of the trivial ambiguities for $\hat{g}$: a)- global phase shift, b)- conjugate inversion, c)- spatial shift, have the same Fourier modulus.

It is known that prior information increases the probability of convergence to the true solution [3]. Then, to initialize the algorithms, we obtain a rough seed by means of a holographic technique [4] and test its consequent benefits. In order to experimentally evaluate the OPR techniques, we propose a simple two beam interferometric setup to recover the object phase and compare it against the phase retrieved by the recursive OPR algorithms. Since the object phase is also interferometrically determined, this gave us the opportunity to introduce the structural similarity index measure (SSIM) to the OPR study framework.

This paper is organized as follows: in Section 2, we briefly describe the compared algorithms based on alternating projections and the criteria for comparison. Section 3 presents the theoretical object to be tested and introduces the framework of the exact complex–wave reconstruction to obtain a rough estimate object used as an initial guess. In Section 4, we show the performances obtained in the phase retrieval problem by using numerical simulations. Section 5 describes the experimental setup and analyzes the results and the different sources of uncertainty when the object phase map is embedded in a micro-channel. In Section 6, a summary and conclusions are offered.

2. Algorithms based on alternating projections

The most popular kind of phase retrieval methods are based on alternating projections. These methods are of low algorithmic complexity and easy application. Thus, they can be used by non-specialized operators. In 1982, Fienup proposed a family of iterative algorithms that are related to different interpretations of the Gerchberg and Saxton method [5,6]. The general framework is the Error-Reduction iterative algorithm (ER), which consists of the following four steps shown in the block diagram of Fig. 1 for iteration n: (1) Fourier transform the object complex signal g_n; (2) make minimum changes in $|G_n|$ to satisfy the Fourier domain constraints and form G'_n; (3) inverse Fourier transform of G'_n; and (4) make minimum changes in g'_n to satisfy the object domain constraints to form a new estimate of the object signal g_{n+1}. An initial guess g_i is commonly given to the iterative process by assigning to each object coordinate location $\mathbf{x} = (x, y) \in \mathbb{R}^2$ a phase composed of uniformly distributed values between $-\pi$ and π. The Fourier constraints are satisfied by replacing $|G_n| = |F|$, where $|F| = \sqrt{I}$ with I the measured intensity in the Fourier domain of the object signal. The object constraints are described as

$$g_{n+1} = \begin{cases} 0 & \{x, y\} \in \gamma, \\ g'_n & \text{otherwise}, \end{cases} \tag{2}$$

where γ includes all points at which the n^{th} estimate of the object function g'_n violates the object extent constraints. We employ the nomenclature proposed in the literature for the reviewed algorithms. In this case, γ is the region in the input object plane where the field values are

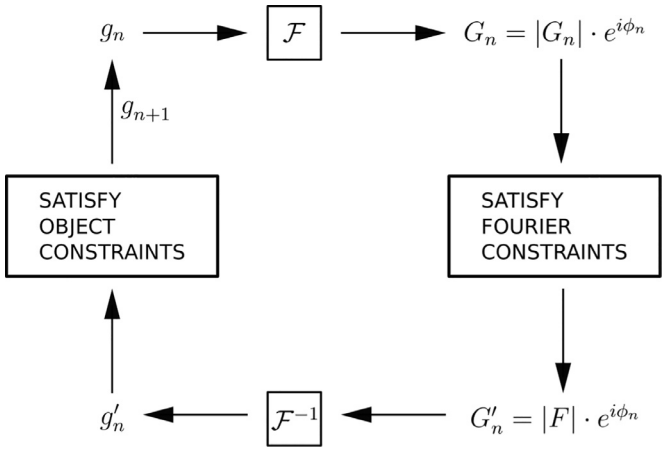

Fig. 1. Block diagram of the ER iterative phase retrieval algorithm.

all zero. One of the most commonly used variant to this ER iterative algorithm is referred to as the Hybrid Input-Output (HIO) method

$$g_{n+1} = \begin{cases} g_n - \beta g'_n & \{x, y\} \in \gamma, \\ g'_n & \text{otherwise}, \end{cases} \tag{3}$$

where β is a constant feedback parameter with values in [0.5, 1]. The HIO algorithm is currently the most widely used algorithm in comparison to the other variants known as the Input-Output (IO) algorithm

$$g_{n+1} = \begin{cases} g_n - \beta g'_n & \{x, y\} \in \gamma, \\ g_n & \text{otherwise}, \end{cases} \tag{4}$$

and the Output-Output (OO) algorithm

$$g_{n+1} = \begin{cases} g'_n - \beta g'_n & \{x, y\} \in \gamma, \\ g'_n & \text{otherwise}. \end{cases} \tag{5}$$

Only the amplitude of the Fourier image and γ are necessary for the object phase recovery. As is known in the specialized literature, some precautions must be taken when applying iterative methods to avoid stagnation, slow convergence and the twin image problem [7]. The combination of the ER and HIO iterative algorithms can perform a better phase retrieval process than separated realizations [8]. To avoid confusion, we name the combination of both a distinct standard iterative method ER/HIO.

As shown in Ref. [9] the combination of the HIO and ER algorithms is significantly outperformed by an extension of this combination based on randomized overrelaxation. The authors show that this extension can enhance the success rate of reconstructions for a fixed number of iterations as compared to reconstructions solely based on the traditional algorithm. We briefly review this algorithm for completeness and name it HIO/O/ER. Therefore, it is convenient to define projection operators P_S and P_A from the operations shown in Fig. 1. It is direct to observe that $g_{n+1} = P_S P_A g_n$ for the ER algorithm. The operator P_A performs the Fourier transformation and conserves the measured amplitude and P_S inverse Fourier transform by fixing the block of zeros corresponding to γ. We encourage the readers to consult Ref. [9] for a proper review. In these terms, HIO is rewritten as $g_{n+1} = [1 - P_S - \beta P_A + (1 + \beta) P_S P_A] g_n$.

The extension of the ER/HIO to the HIO/O/ER is based on overrelaxation and randomization. The authors replace the projection operator P_A by the relaxed expression $L = 1 + \lambda_A (P_A - 1)$ obtaining a new expression for the HIO with overrelaxation $g_{n+1} = [1 - P_S - \beta L + (1 + \beta) P_S L] g_n$, where λ_A is a real constant called relaxation parameter. To include the randomization, in each iteration λ_A is randomly selected with a uniform distribution within a given range of specific values. Formally, the authors present a framework for studying randomization of any iterative projection algorithm and limit its use to parameter values whose deterministic contribution coincide with the HIO algorithm. In this framework, a projection polynomial operator is considered, and by means of

a working hypothesis, the following expression for the HIO with randomized overrelaxation is obtained:

$$g_{n+1} = [b\ 1 + c_{S,1}P_S + c_{A,1}P_A + c_{S,2}P_SP_A + c_{A,2}P_AP_S]g_n, \tag{6}$$

with the constraint

$$b = 1 - \sum_{n=1}^{2}(c_{S,n} + c_{A,n}), \tag{7}$$

and the following coefficients

$$c_{S,1} = -1 - \gamma_A(1+\beta), \tag{8a}$$

$$c_{A,1} = -\beta(1+\gamma_A), \tag{8b}$$

$$c_{S,2} = (1+\beta)(1+\gamma_A), \tag{8c}$$

$$c_{A,2} = 0, \tag{8d}$$

where γ_A is uniformly distributed in $[-\nu, \nu]$ and $\nu \approx 0.5$. Finally, the ER algorithm is applied to complete the iterative process HIO/O/ER (see Fig. 1 in Ref. [9] for a graphical illustration of the HIO/O/ER algorithm and its building blocks).

The twin image problem is a drawback when using iterative algorithms. The obtained estimate often stagnates and contains the features of the ideal solution and its inverted and complex-conjugated replica. This drawback is more severe when the object support is centrosymmetric. Recently, an important observation was made: the ideal solution without the twin image is typically more sparse in some suitable transform domain as compared to the stagnated solution [10]. This observation facilitated the construction of a new method based on the introduction of a sparsity–enhancing step in the iterative algorithm without the need to change the object support throughout the iterative process, even when the object support is centrosymmetric. Following, we briefly describe the modified version of the HIO algorithm incorporating a sparsity–enhancing step with the functional gradient of the Huber penalty, named HIO/TV. From Ref. [10], the HIO/TV algorithm computes an estimate in the n^{th} step by applying the HIO method. Then, a new solution is updated by using a fixed number N_{TV} of gradient descent steps k of the following form for TV reduction

$$g'^{k+1}_{n+1} = g'^{k}_{n+1} + \frac{t}{2\delta^2}\nabla \cdot \left(\frac{\nabla f}{\sqrt{1 + \frac{|\nabla f|^2}{\delta^2}}} \right), \tag{9}$$

where $f = g'^{k}_{n+1}$ and the step size t is determined in each iteration by a backtracking line search. δ is a running parameter elected as the median of the gradient magnitudes over all object coordinates in each gradient descent step.

2.1. Convergence and quality criteria

With the purpose of examining the convergence properties of the above algorithms, it is convenient to define a numerical tool before introducing the different comparisons of numerical simulations. In phase retrieval, the iterations continue until the computed Fourier transform satisfies the Fourier domain constraints and an estimate is found. Then, we say that the associated Fourier transform pair satisfies all the constraints in both domains for that estimate and with a determined convergence error. The convergence error is usually evaluated by means of the discrete sum of squared errors (*SSE*)

$$SSE(n) = 10\log\left\{ \frac{\sum_{j=1}^{J}\sum_{k=1}^{K}\left[|G_n(j,k)| - |F(j,k)|\right]^2}{\sum_{j=1}^{J}\sum_{k=1}^{K}|F(j,k)|^2} \right\}, \tag{10}$$

where J and K are the dimensions of the image corresponding to the measured intensity in the Fourier domain. Note that *SSE* provides partial information and it is also difficult to interpret as a quality index associated with the retrieved phase map. However, it is found in literature as a common procedure and we included it with the aim of showing an additional reference for comparison purposes with other authors.

In order to investigate the quality Q of the recovered phase map, we evaluate the structural similarity index measurement (SSIM) [11]. The distortion measured by the SSIM index is associated with loss of correlation, undesired offset of the mean phase, or modification of the standard deviation. We adopt this form of SSIM index

$$Q_j = \frac{(2\overline{\phi}_A\overline{\phi}_B + C_1)(2\sigma_{\phi_A\phi_B} + C_2)}{(\overline{\phi}_A^2 + \overline{\phi}_B^2 + C_1)(\sigma_{\phi_A}^2 + \sigma_{\phi_B}^2 + C_2)}, \tag{11}$$

where ϕ_A and ϕ_B are the phase images being compared, $\overline{\phi}$ is the mean value of ϕ, σ is the standard deviation, and $\sigma_{\phi_A\phi_B}$ is the correlation coefficient between ϕ_A and ϕ_B. C_1 and C_2 are small positive constants that avoid numerical instability for near zero sample means, standard deviations or correlation coefficients. $C_1 = 0.01$ and $C_2 = 0.03$ were chosen to obtain comparable results. $Q \in [-1, 1]$ and $Q = 1$ is satisfied for exact phase recovery. We calculate Q as the mean value of several Q_j of locally obtained SSIM indices using a sliding window approach.

It is important to stress that for the numerical and theoretical analysis of OPR algorithms, the object phase can be known and both criteria (SSIM and SSE) can be applied in order to evaluate the performance. However, the object phase is generally unknown in real experiments and the application of the SSIM index is not possible. In Section 5, we propose a simple interferometric optical setup for experimental evaluation and testing of OPR algorithms. Note that unlike the SSE, the SSIM index compares the retrieved phase against the original phase. According to our knowledge, this methodology is first demonstrated in Section 4 by numerical examples and in Section 5 by experimental measurements. There, we show the importance of evaluating and analyzing the OPR algorithms with the SSIM index. In the following section we describe the basic geometry of the object under study and the object support. This leads us to implement a coarse holographic technique in order to produce a rough estimate of the object that favors the numerical convergence. This allows us to analyze the OPR algorithms when they are assisted by an initial guess.

3. Phase retrieval layout and a rough seed implementation obtained by holographic combination

We are concerned with the performance comparison of alternating projection methods, as described in the preceding section. Although the application of these methods does not require specialized operators, these methods often fail to work. Therefore, we believe that it is necessary to rethink the object support and the introduction of an initial guess for a proper recovery of the phase fields. We implemented an object geometry that offers the possibility to find a rough seed by means of a coarse holographic technique and use it for initialization of the OPR algorithms. The proposed geometry is extremely simple and suggests the proof of concept of a refractive index sensor.

3.1. Object signal description

We analyze the OPR process by transmission through a centrosymmetric object support. The presence of this symmetry in the object support contributes to the problem of twin image [7]. However, it is our intention to show the behavior obtained during the process of OPR for an unfavorable condition.

We begin our theoretical comparison with a theoretical object function as shown in Fig. 2. The circular aperture represents a signal object immerse in γ where we distinguish two different regions: a reference aperture (*AP*) and the test object (*OB*), both of the same size. In

one-half (*AP*), we form a reference aperture, which is simply left as an empty space for the introduction of the holographic approach. In the other (*OB*), we introduce the proper unknown object signal to be determined by transmission. In Section 4 the numerical experiments deal with a highly artificial but challenging test object *OB* (the object phase is given by the standard test Lena image). In Section 5 we perform the experimental phase retrieval evaluation by placing a micro-channel as a test object.

3.2. A rough seed obtained by holographic combination

A holographic scheme can be introduced in the optical setup used in the phase retrieval problem with the aim of producing a rough seed [12]. It is well known that the introduction of a tiny hole at a predetermined position in the object plane creates an additional wave with a tilted phase. This mechanism allows the introduction of additional information which is used for increasing the resolution of the algorithmic recovery or for relaxing the constraints on the prior knowledge of the object support (see Ref. [3] and reference therein for successful applications combining a holographic procedure). A systematic evaluation of the importance of approximate Fourier phase information for the phase retrieval problem can be consulted in Ref. [13]. In this reference, the authors discover that a rough phase estimate up to $\pi/2$ enables the development of efficient algorithms whose reconstruction time is an order of magnitude faster than HIO.

We base our argument in the framework of the exact complex-wave reconstruction applied in digital holography [4]. A hologram is formed by the spatial superposition of two mutually coherent waves. In our case, one wave comes from the object (*OB*) named E_o, and the other emanates from the reference aperture (*AP*) E_r. Note that E_r is introduced with a direction $\mathbf{k}_r$, thus $E_r = A\exp(-i\mathbf{k}_r\cdot\mathbf{x})$, where A and $\mathbf{k}_r$ are the complex amplitude and wave-vector respectively, and $\mathbf{x}$ corresponds to the coordinates of a point in space. Then, the interference pattern to be analyzed is constructed and specified as $I(\mathbf{x}) = |E_r + E_o|^2$, where E_o is the object field to be determined and $I(\mathbf{x})$ is the spatial intensity distribution measured at the CCD sensor. From Theorem 1 in Ref. [4], the following identity

$$\mathcal{F}\left[\ln\left(1+\frac{E_o}{E_r}\right)\right] = \mathcal{F}\left[\ln\left(\frac{I}{|E_r|^2}\right)\right]\mathbf{1}_{[0,+\infty)\times[0,+\infty)} \tag{12}$$

is verified when the Fourier transform $\mathcal{F}[E_o/E_r]$ is identically zero outside of the quadrant of the frequency domain given by $[0,+\infty)\times[0,+\infty)$ and $|E_o/E_r|<1$. The knowledge of the interferogram cepstrum in Eq. (12) exactly recovers the object field E_o by the inversion of the Fourier transform and the use of the exponential function

$$E_o = \left[\exp\left(\mathcal{F}^{-1}\left\{\mathcal{F}\left[\ln\left(\frac{I}{|E_r|^2}\right)\right]\mathbf{1}\right\}\right) - 1\right]E_r. \tag{13}$$

Note that $|E_r|^2$ is measured blocking *OB*, whereas E_r can be either estimated or measured. When the angle between the wave vectors corresponding to the object and reference is large, Eq. (13) shows high performance. In Fig. 2, the reference wave is realized by the reference aperture (*AP*). This way, the presented object does not have the beforementioned condition (the angle value is very low in this case). Therefore, the recovered object field is unsatisfactory. However, this roughly obtained approximation of the object field can serve as an initial guess (rough seed) when using alternating projection methods and improves the convergence and accuracy of the solution.

4. Comparisons of numerical simulations

We analyze and discuss the results for different object considerations and seeds in order to compare different phase retrieval algorithms. For this comparison, we employ a highly artificial object (Fig. 2). In the object area (*OB*) the amplitude is characterized by a random uniform distribution in the interval [0, 1] whereas the phase is given by the known Lena image as a phase map in $[-\pi,\pi)$. In the reference aperture (*AP*) we define a uniform field $4\exp(i\pi/4)$. γ is a block of zeros as shown in Fig. 2(a). The size of the images considered (Fig. 2) is 512×512 pixels and the evaluated object occupies a circle of 256 pixels of diameter. Therefore, the object under test is quite challenging since it is centrosymmetric with random amplitudes and a phase map of very fine details.

- Case **I**. No prior knowledge is considered on either the object region *OB* or the aperture region *AP*. Therefore, the seeds to support the algorithms are fields of unitary amplitudes and random phases in $[-\pi,\pi)$.
- Case **II**. No prior knowledge is considered on the region *OB*. In this case the seeds are divided into the two regions (*OB* and *AP*). The initial guess at region *OB* is fed with a uniform amplitude and random phases in the interval $[-\pi,\pi)$. In the region *AP*, the seed is an intentionally untrue but uniform value of amplitude and phase.
- Case **III**. No prior knowledge is considered on the region *OB*. However, since we a priori know the complex field of the reference aperture and the Fourier spectrum intensity of the object and the aperture jointly (*I*), we obtain an initial guess for *OB* from Eq. (13).

Below, we show the results obtained by means of the different algorithms described in Section 2 and the OPR layout described in Section 3. We also analyze and discuss the most important sources of uncertainty.

4.1. Comparisons obtained in cases I and II

The comparisons between Case **I** and Case **II** should offer an idea about the use of these alternating projection algorithms working directly on a straightforward problem of phase retrieval (i.e. a complex object immersed in a centrosymmetric support by adopting an oversampling of 2). In order to highlight the results obtained for a proper analysis, we employ a common numerical procedure for FFT calculations and a non quantized Fourier spectrum.

We are interested in retrieving the phase of the object g_o shown in Fig. 2. Fig. 3 shows the results obtained using the HIO/O/ER algorithm with 5 cycles of 30 and 100 iterations for HIO/O and ER, respectively, and $\beta = 0.9$ and $\nu = 0.3$. As the object phase is exactly known in the numerical simulations, then we can use the *Q* index for the evaluation of the recovered phase. In Fig. 3(a–d), we show the results of *SSE* and *Q* corresponding to 16 trials using two different kinds of seeds. Case **I**: Fig. 3(a) and (b) depict the results for seeds with random phases in $[-\pi,\pi)$ and unitary amplitudes. Case **II**: Fig. 3(c) and (d) depict the case when the seeds are divided into two zones. The region *OB* (Lena place) is fed with seeds of random phases in $[-\pi,\pi)$ and unitary amplitude, whereas the region *AP* (reference aperture) is filled with a uniform seed of amplitude 4 and phase $\pi/2$. In Fig. 3(a–d) the beginning of each cycle is noticeable every 130 iterations (a similar behavior can be observed in Ref. [8]). Whereas *SSE* shows that the convergence slightly improves after each cycle, the *Q* index, which compares the retrieved phase against the original, shows no significant tendency. According to *SSE* (Fig. 3(a) and (c)), the convergence obtained in Case **II** trials does not present significant improvement when compared to Case **I** trials. However, according to the *Q* index (Fig. 3(b) and (d)) the convergence obtained evidences a little improvement for Case **II** trials. In these comparisons we do not analyze the degradation of the recovered phase due to the reduction of the quantization levels, since the algorithms tested already exhibit a poor performance.

According to our experience, none of the algorithms presented in Section 2 was able to improve the results of Fig. 3 and therefore this behavior can be considered representative for the analysis. We emphasize that the alternating projection algorithms under the conditions of Case **I** and Case **II** are hard to manage. The algorithms require operating with proper parameters to be successful and therefore an exhausted search must be implemented. In these comparisons, we did not find significant results even though we tested a wide set of parameters for all algorithms presented. We conclude that it is important to possess a set of

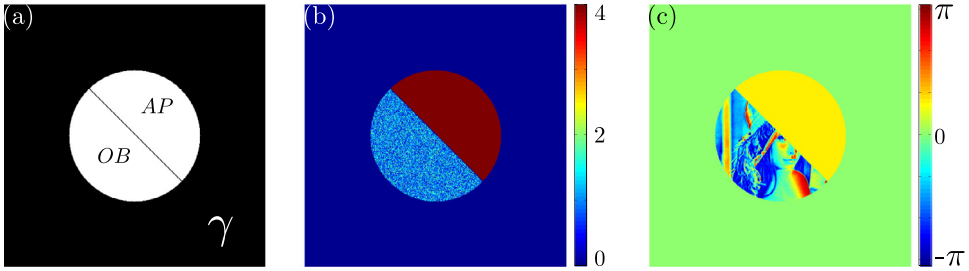

Fig. 2. (a) Schematic diagram of the forming parts of the object signal g_o (*OB* and *AP*) and γ. Numerical simulation (b) Amplitude of the object $|g_o|$: at *OB* random uniform distribution in the interval [0, 1], and at *AP* constant amplitude of 4. (c) Phase of the object $\angle(g_o)$: at *OB* Lena image in the interval $[-\pi, \pi)$ rad, and at *AP* constant phase of $\pi/4$.

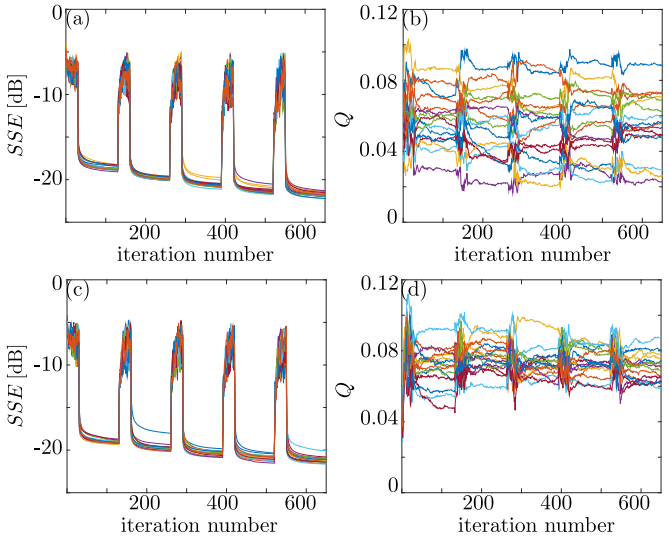

Fig. 3. *SSE* and *Q* obtained for the object depicted in Fig. 2 using the HIO/O/ER algorithm (16 different trials) with 5 cycles of 30 and 100 iterations for HIO, O, and ER, respectively (i.e. a total of 650 iterations). $\beta = 0.9$ and $\nu = 0.3$. (a) and (b) correspond to seeds with unitary amplitude and random phases in $[-\pi, \pi)$ (Case **I**). (c) and (d) correspond to seeds that are discriminated into the reference aperture (*AP*) and the object zone (*OB*) (Case **II**). In *AP*, the initial guess is uniform $g_i = 4\exp(i\pi/2)$. In *OB* the initial guess corresponds to random phases in $[-\pi, \pi)$ and unitary amplitude.

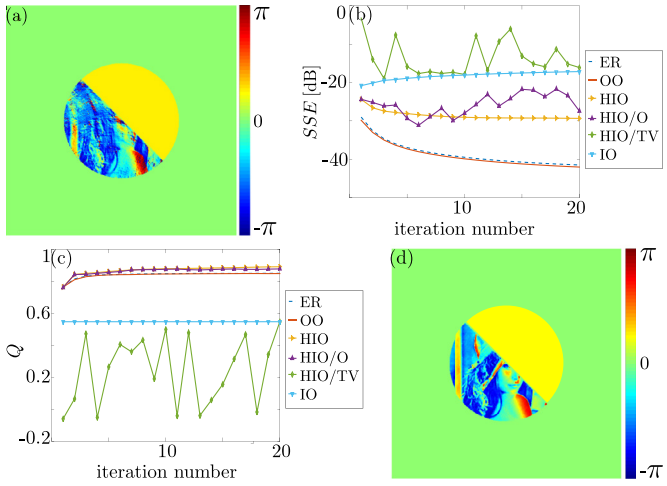

Fig. 4. (a) Seed obtained from Eq. (13) and E_r. (b) *SSE* and (c) *Q*, obtained for 6 different algorithm implementations (1 trial) along only 20 iterations. (d) Final result after 5 iterations using HIO. The values of the algorithm parameters were $\beta = 0.9$ and $\nu = 0.5$.

parameters to alleviate the external operator task. We believe that finding proper conditions in the test object that facilitate the phase recovery procedure can be an alternative. According to our experience, it is not possible to recover the object phase in these cases with a centrosymmetric support and wide range Fourier spectrum (Fig. 3). However, some prior knowledge on the test object g_o allows us to modify the initial seed and minimally improve the performance of the algorithms (Fig. 3(d)). This tendency is observed in all of the algorithms under test.

4.2. Comparisons obtained in case **III**

In this case, we firstly consider having a perfect reference wave (*AP*). Therefore, by means of Eq. (13), a seed (Fig. 4(a)) is determined and it feeds the different algorithms. We assume that the magnitude of the Fourier spectra corresponding to the reference aperture $|E_r|^2$, and the object and the aperture jointly (I) are both quantized in 2^{32} levels. This quantization is considered as a large dynamic range and leads to the improvement of OPR using iterative Fourier transform algorithms [14]. Fig. 4(b) and (c) resume the results obtained after only 20 iterations for each algorithm according to *SSE* and *Q*, respectively. According to Fig. 4(b), for ER, OO, and HIO, *SSE* decreases along with the number of iterations. However, after three iterations the quality index *Q* does not present significant variations (Fig. 4(c)) and no improvement is reached in the final phase map. According to the *Q* index (Fig. 4(c)) ER, OO, HIO, and HIO/O present a similarly good performance whereas IO presents a less efficient performance. Fig. 4(d) shows the final result after 5 iterations using HIO. The values of the algorithm parameters are $\beta = 0.9$ and $\nu = 0.5$. Note that in order to find a satisfactory object phase field, less than five iterations might be sufficient.

An important observation in the use of these alternating projection algorithms is that no important deviations should be found in the output results for a minimum variation of the operating parameters of the algorithm [15]. However, in our experience, HIO/TV is very sensitive and hard to manage (Fig. 4(c)).

As stated before, it is important to know the degradation of the performance when the quantization levels are reduced. We still find efficient performances for ER, OO, and HIO when decreasing the quantization scale down to 2^{24} levels (Fig. 5(a)). HIO/O required a few iterations more in order to obtain the same performance as before. According to our experience, the alternating projection methods give degradable results if the acquisition of images has less than 2^{24} levels of quantization.

It is also convenient to consider the situation where the field associated to the reference beam is not precisely known (i. e. when the reference wave is imprecise) [16]. Thus, we maintain the quantization in 2^{24} levels but we test a new seed. In the reference aperture zone *AP* the field is now defined numerically as a constant of amplitude 1 and null phase values uniformly distributed. However, the Fourier spectra for the object I and the reference wave $|E_r|$ are considered as known. Thus, Eq. (13) is applied in order to obtain a new seed from an improper reference wave. Fig. 5(b) shows how this seed affects the performance

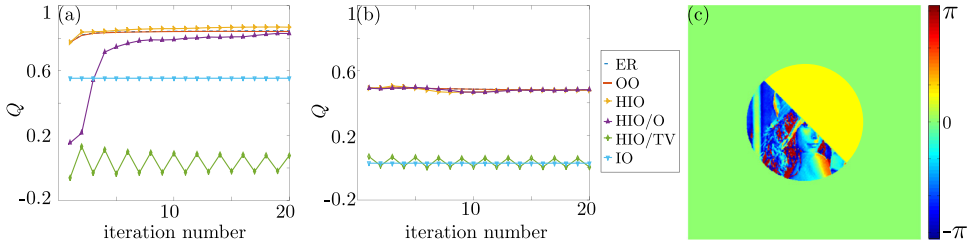

Fig. 5. (a) Results of Q obtained for each algorithm in the same conditions as Fig. 4 and using a quantization scheme of 2^{24} levels instead of 2^{32}.(b) Results of Q obtained for each algorithm in the same conditions as (a) but the seed is defined numerically as a constant of amplitude 1 and null phase values uniformly distributed in the reference aperture zone. (c) The recovered phase map for HIO method in 5 iterations.

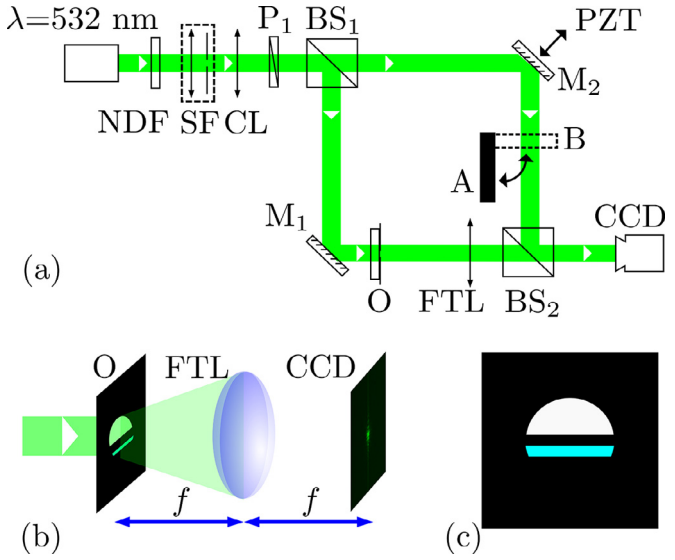

Fig. 6. Experimental setup. (a) Scheme of the experiment. 532 nm laser. NDF: Neutral density filter. Spatial filter (SF) formed by a microscope objective and a pinhole. CL: collimating lens; P_1: polarizer BS: beam splitters; O: test object CCD: digital camera attached to a computer. FTL: Fourier transform lens. PZT: piezo–electric actuator. Shutter A: the reference arm is available for interferometry. Shutter B: the reference arm is blocked for phase retrieval. (b) Experimental setup for phase retrieval (Mach–Zehnder test arm). f: 150 mm focal length. (c) Experimental test object (object signal g_o). Object support: 4 mm circular perforation on a steel plate. Aperture (*AP*): empty space (upper region). Object (*OB*): 500 μm wide channel filled with a thin cellophane layer (lower region).

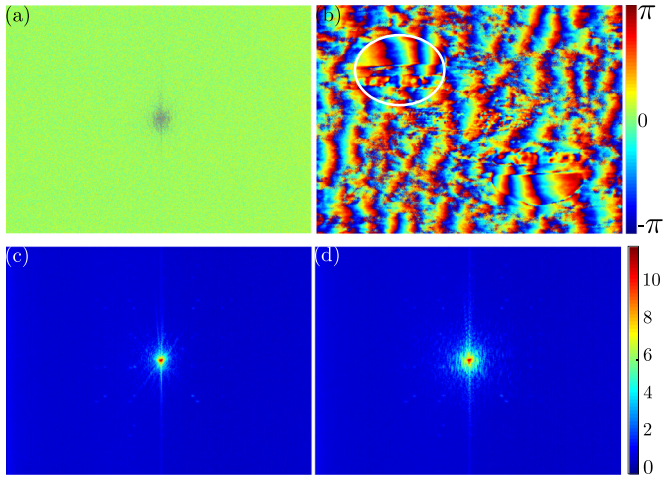

Fig. 7. Phase maps and Spectra (1040 × 1392 pixels). (a) Phase map of the measured spectrum by the PSI procedure (radians). (b) Phase map of $\hat{g}_{PSI}$ obtained from (a) by applying a numerical inverse Fourier transform procedure (radians). (c) Fourier spectrum intensity measured for the reference aperture zone only, $|E_r|^2$ (logarithmic scale). (d) Fourier spectrum intensity measured for the complete object (micro–channel and aperture zones simultaneously), I (logarithmic scale).

of the different algorithms. ER, OO, HIO, and HIO/O obtain a distorted phase map but Lena's face is still easily recognized after a few iterations (Fig. 5(c)). These algorithms are quite robust for variations of the reference amplitude $|E_r|$ but they introduce a severe distortion in the retrieved phase.

The numerical evaluation of the algorithms shows that the *SSIM Q* index provides a more accurate description than the *SSE*. According to the Q index, the reduction of the *SSE* after each cycle has no practical impact on the quality of the object phase recovered. Although the object support is centrosymmetric, the results found for Case **III** suggest that the alternating projection algorithms can still exhibit a good performance according to the OPR layout proposed (Section 3), if two features are achieved: (1) enough quantization levels in the acquisition of the spectra are employed, and (2) a rather accurate reference wave is known. Therefore, the following sections present the experimental development and analysis for Case **III**.

5. Experimental procedure

In order to test the results of OPR methods, we propose a two beam interferometric setup. This scheme allows us to evaluate the OPR results by means of the Q index. Note that both techniques are implemented in the same experimental scheme: the OPR procedure uses only one arm of the interferometer (test arm) whereas the interferometric procedure uses both arms.

The experimental setup is based on a Mach–Zehnder interferometer as depicted in Fig. 6(a). We add a lens to the test arm to produce the Fourier transform of the object complex signal. This way, the test arm projects the Fourier transform of the object on the plane of the detector. This optical system also allows us to find one of the most direct real-space constraints, often known as the object support, which is a source of uncertainty in the phase recovery procedure.

The light source is a diode pumped solid state laser of wavelength $\lambda = 532$ nm that is attenuated by a neutral density filter (NDF). The main beam is expanded and spatially filtered by an optical set (SF) composed by a 10*X* microscope objective, a pinhole of 10 μm and a collimating lens (CL). The polarization of the main beam is adjusted by a polarizer (P_1) and subsequently split into two secondary beams (named test and reference beams) using a beam splitter (BS_1). The test beam of the interferometer traverses the transmissive object (O) that constitutes the object signal g_o. It is followed by a 25 mm diameter lens (FTL) of a focal length of 150 mm that produces the Fourier transform of the complex-valued test object transmittance F in its back focal plane where a CCD is placed (Fig. 6(b)). The intensity measurements are performed with a charge-coupled device camera (CCD) of 1040 × 1392 pixels and with a pixel size of 6.45 μm × 6.45 μm (QIClick-1392). The test object consists of a 4 mm circular aperture on a steel plate (Fig. 6(c)) which is

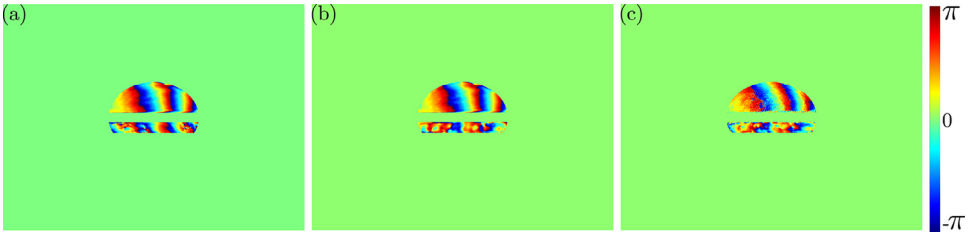

Fig. 8. Phase maps (radians, 1040 × 1392 pixels). (a) Seed obtained using Eq. (13) and Fig. 7(c)–(d). (b) Object phase map, $\hat{g}_{PSI}$ recovered using PSI technique. (c) Object phase map recovered using HIO/O and ER with 4 cycles of 10 and 100 iterations, respectively, and $\beta = 0.9$ and $\nu = 0.5$.

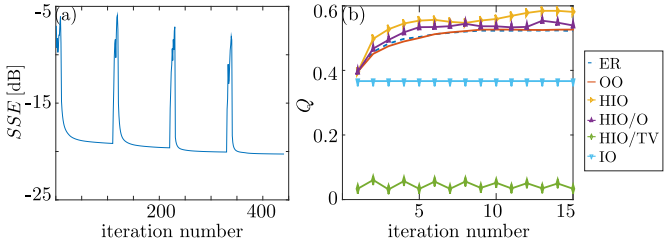

Fig. 9. (a) *SSE* for HIO/O and ER with 4 cycles of 10 and 100 iterations, respectively, and $\beta = 0.9$ and $\nu = 0.5$. (b) *Q* obtained for each algorithm when the quality index is only considered in the micro-channel. Comparison between the phase maps obtained by PSI technique and the different recursive algorithms.

divided into two regions. The upper region of g_o is an empty aperture (*AP*) whereas the lower region (*OB*) has a test channel. This channel is 500 μm wide and filled with a thin cellophane layer. The reference beam is reflected by a piezoelectrically actuated mirror (M_2) and recombined with the test beam by means of a beam splitter (BS_2). This optical arrangement allows us to apply a four–step phase–shifting interferometric (PSI) technique, measure the complex-valued Fourier transform of the test object *F*, and backpropagate it to the object plane in order to obtain $\hat{g}_{PSI}$. This way, the experimental setup allows us to determine the optical phase spread over the object plane. Therefore, the results obtained by means of OPR methods can be compared with those from the PSI technique by means of both criteria: the *SSE* and the *Q* index. In order to acquire the spectra *I* and $|E_r|^2$, we only use the test arm of the Mach–Zehnder interferometer, while we block the reference arm. This way, we use the same experimental setup for both techniques.

5.1. Interferometric procedure

The measurement process for the recovery of the object phase is based on a very well known four-step PSI technique [17]. We take four phase-shifted interferograms corresponding to the superposition of the fields associated with the test and the reference arms by introducing a phase angle difference via the piezoelectrically actuated mirror M_2. With this procedure, the complex-value of the Fourier spectrum *F* is measured. Fig. 7(a) shows the phase map of the measured spectrum $\angle F$. The object signal $\hat{g}_{PSI}$ is reconstructed by back–propagating the recovered complex fields (amplitude and phase) to the object plane by the inverse Fourier transform. Note that this interferometric procedure allows us to know the reference wave E_r, which is necessary to implement Eq. (13) and determine an initial guess. Fig. 7(b) illustrates the phase map corresponding to $\hat{g}_{PSI}$, which is obtained from Fig. 7(a) by applying a numerical inverse Fourier transform procedure. Note that the boundary of the object g_o is easily determined and therefore the object support can be specified to assist the phase retrieval process. We complete the boundary with blocks of zeros in order to obtain the image format corresponding to the CCD employed in the measurement (1040 × 1392).

5.2. Phase retrieval procedure

In order to obtain an initial guess (by means of Eq. (13), the measurement process for phase retrieval proposed in Section 3 involves the acquisition of two Fourier spectrum images separately. One corresponds to $|E_r|^2$, the Fourier transform of the reference aperture (*AP*) located in the upper region of the object g_o, whereas *OB*, the lower region (micro-channel), is blocked (see Fig. 6(c)). The other image corresponds to *I*, the Fourier transform of the complete object g_o (upper region and lower region uncovered).

It is important to note that the first image corresponding only to the empty aperture remains unaltered whereas the space corresponding to the lower region may change due to the test object deposited in the 500 μm channel (e. g. a test object with a dynamic phase). Since the aperture remains unaltered for different test objects immersed in the micro-channel, there is no need to repeat the first image. Moreover, this millimeter size semicircular slit is very easy to reproduce experimentally and this step should not be considered as a severe design problem.

5.2.1. High dynamic range imaging

As discussed in Section 4, the quantization error in the measurement of the Fourier spectrum for the phase retrieval process leads to an important error in the reconstructed object. Thus, an alternative to reduce this source of uncertainty is necessary. In this work, we improve the performance of phase retrieval methods by adopting an approach based on the High Dynamic Range Imaging (HDRI) technique [18]. We acquire a sequence of 200 images with a linear incremental exposure time starting at 12 μs with 12 μs increments. The exposure time and laser power are adjusted in order to obtain a sequence of intensity growing images that starts without any saturated pixels. By using a model of linear regression, the intensity of each pixel is linearly estimated as a function of the exposure time, and the dynamic intensity range is then expanded.

Fig. 7(c) and (d) show, in logarithmic scale, the intensities measured for the reference aperture Fourier spectrum only, $|E_r|^2$, and the complete object Fourier spectrum, *I* (micro-channel and aperture zones simultaneously), respectively. Both images were obtained by using the previously described HDRI procedure adopting a format of 1040 × 1392 pixels. The condition $I > I_r$ required for using Eq. (13) is clearly verified. Fig. 7(c) characterizes the reference wave via the Fourier transform $|E_r|^2$. This is substituted in Eq. (13) to obtain an initial guess (Fig. 8(a)).

5.3. Experimental comparisons

We compare the performance of the different phase retrieval methods based on the same experimental measurements as described in Fig. 7. To verify the results obtained and carry out a quantitative comparison, we compare the results obtained by using the different phase retrieval methods against the PSI measurement. Fig. 8(c) shows the phase map of the complete object (reference aperture and micro–channel) recovered. Fig. 8(b) illustrates the phase map of the object $\hat{g}_{PSI}$, which is obtained by employing the PSI technique. Fig. 8(a) shows the seed obtained following the procedure described. Note that the seed phase map corresponding to the micro-channel is different from the original

Fig. 8(b). In this case, we utilize the HIO/O and ER with 4 cycles of 10 and 100 iterations, respectively. The parameters for the algorithm are $\beta = 0.9$ and $\nu = 0.5$. Fig. 9(a) shows its performance according to *SSE*. We use the phase map of the micro–channel, known via an interferometric procedure, as the reference in the quality index SSIM calculation (Eq. (11)). As in the previous examples, increasing the number of iterations does not improve the final recovered phase map. Fig. 9(b) summarizes the results for Q index found in the comparisons. Only a few iterations are necessary for the ER, OO, HIO, HIO/O algorithms to achieve a relative stagnation. The best value obtained is not higher than $Q = 0.6$ and the recovered phase of the micro–channel can be observed in Fig. 8(c).

Not only do these experimental results agree with the numerical results (Section 4), but they also demonstrate the advantage of the proposed OPR evaluation scheme.

6. Conclusions

The phase retrieval problem is not convex, and the solution depends on the initialization and on the complex object signal. Moreover, there is no guarantee that a solution can be found algorithmically. However, phase retrieval is still appealing since it does not require interferometric optical setups. It is also attractive for the characterization of test objects by simple free propagation and record of its Fourier spectrum in amplitude. Therefore, all possible alternatives that seek to combine prior information are useful to face these difficulties. In addition, systematic evaluations of phase retrieval methods are necessary to identify the most important sources of uncertainty involved and redirect the experimental efforts.

Throughout this work, we have shown the importance of quantization levels and how detrimental a centrosymmetric support can be. However, both experimental conditions can be overcome by means of a simple reference aperture in the object domain and an increased quantization. The latter generates a severe trade-off between the characteristic time of the dynamics of the object phase and the exposure time required to implement a process of HDRI. The insertion of an aperture in the object domain allows us to introduce an initial guess, which improves the phase retrieval. Although it is necessary to know the reference wave, we show that it is possible to retrieve the phase in only a few iterations. This approach can be very useful because the reference wave is measured only once. Moreover, the reference wave associated with a semicircular aperture is easily reproducible.

Convergence properties of the alternating projection methods are usually examined by means of *SSE*. However, we show that *SSE* is not a good measure when compared to the quality index Q associated with the object phase map recovered, which is the variable of concern. The Q index allows us to identify the importance of the quantization levels and the use of an initial guess. Moreover, according to the Q index, the algorithms ER, OO, HIO, and HIO/O offer similar performances and are followed by IO. All of these alternating projection methods are not very sensitive to external parameters. However, HIO/TV proves to be more demanding and requires working with a trained external operator.

We also evaluate the experimental use of alternating projection methods in the phase retrieval process corresponding to a micro-channel in a transmissive way. A dedicated optical setup based on a Mach–Zehnder interferometer with the possibility of measuring the object phase using PSI was implemented to compare the results obtained. Due to the proven efficiency of interferometric techniques, there is no need to rely on costly micro-fabrication processes or electronic microscope facilities in order to guarantee the phase features of the test objects under study.

We experimentally find that the alternating projection methods cannot surpass a value of $Q = 0.6$, even by using a rough initial seed estimated from a precisely known reference wave (considering the object phase measured by PSI as the most precisely determined one). In our experience, when the reference wave is imprecise, the alternating projection methods seem to be less sensitive to amplitude than to phase variations, even though the final Q value is degraded.

References

[1] Guo C, Shen C, Tan J, Bao X, Liu S, Liu Z. A robust multi-image phase retrieval. Opt Lasers Eng 2018;101:16–22.
[2] Guo C, Wei C, Tan J, Chen K, Liu S, Wu Q, Liu Z. A review of iterative phase retrieval for measurement and encryption. Opt Lasers Eng 2017;89:2–12.
[3] Shechtman Y, Eldar YC, Cohen O, Chapman HN, Miao J, Segev M. Phase retrieval with application to optical imaging: a contemporary overview. IEEE Signal Process Mag 2015;32(3):87–109.
[4] Seelamantula CS, Pavillon N, Depeursinge C, Unser M. Exact complex-wave reconstruction in digital holography. J Opt Soc Am A 2011;28(6):983–92. doi:10.1364/JOSAA.28.000983.
[5] Fienup JR. Phase retrieval algorithms: a comparison. Appl Opt 1982;21(15):2758–69. doi:10.1364/AO.21.002758.
[6] Fienup JR. Reconstruction of a complex-valued object from the modulus of its fourier transform using a support constraint. JOSA A 1987;4(1):118–23.
[7] Guizar-Sicairos M, Fienup JR. Understanding the twin-image problem in phase retrieval. J Opt Soc Am A 2012;29(11):2367–75. doi:10.1364/JOSAA.29.002367.
[8] Guo C, Liu S, Sheridan JT. Iterative phase retrieval algorithms. i: optimization. Appl Opt 2015;54(15):4698–708. doi:10.1364/AO.54.004698.
[9] Köhl M, Minkevich AA, Baumbach T. Improved success rate and stability for phase retrieval by including randomized overrelaxation in the hybrid input output algorithm. Opt Express 2012;20(15):17093–106.
[10] Gaur C, Mohan B, Khare K. Sparsity-assisted solution to the twin image problem in phase retrieval. J Opt Soc Am A 2015;32(11):1922–7.
[11] Wang Z, Bovik AC, Sheikh HR, Simoncelli EP. Image quality assessment: from error visibility to structural similarity. IEEE Trans on Image Process 2004;13(4):600–12.
[12] Latychevskaia T, Longchamp J-N, Fink H-W. When holography meets coherent diffraction imaging. Opt Express 2012;20(27):28871–92. doi:10.1364/OE.20.028871.
[13] Osherovich E, Zibulevsky M, Yavneh I. Approximate fourier phase information in the phase retrieval problem: what it gives and how to use it. J Opt Soc Am A 2011;28(10):2124–31.
[14] Yang S, Takajo H. Quantization error reduction in the measurement of fourier intensity for phase retrieval. Jap J Appl Phys 2004;43(8S):5747.
[15] Fienup JR. Phase retrieval algorithms: a personal tour. Appl Opt 2013;52(1):45–56. doi:10.1364/AO.52.000045.
[16] Osherovich E.. Numerical methods for phase retrieval. arXiv preprint arXiv:12034756 2012.
[17] Rastogi P, Hack E. Phase Estimation in Optical Interferometry. CRC Press; 2014.
[18] Reinhard E, Ward G, Pattanaik S, Debevec P. High dynamic range imaging. data acquisition, manipulation, and display. 2005.